Shared High Value Research Resources: The CamCAN Human Lifespan Neuroimaging Dataset Processed on the Open Science Grid

Don Krieger
Neurological Surgery
University of Pittsburgh
Pittsburgh, PA, USA
kriegerd@upmc.edu

Paul Shepard
Physics and Astronomy
University of Pittsburgh
Pittsburgh, PA, USA
shepard@pitt.edu

Ben Zusman
Neurological Surgery
University of Pittsburgh
Pittsburgh, PA, USA
zusmanbe@upmc.edu

Anirban Jana
Pittsburgh Supercomputing Center
 Pittsburgh, Pa
anirbanjana@cmu.edu

David Okonkwo
Neurological Surgery
University of Pittsburgh
Pittsburgh, PA, USA
okonkwodo@upmc.edu

Abstract—**The CamCAN Lifespan Neuroimaging Dataset [1,2], Cambridge (UK) Centre for Ageing and Neuroscience, was acquired and processed beginning in December, 2016. The referee consensus solver deployed to the Open Science Grid [3,4] was used for this task. The dataset includes demographic and screening measures, a high-resolution MRI scan of the brain, and whole-head magnetoencephalographic (MEG) recordings during eyes closed rest (560 sec), a simple task (540 sec), and passive listening/viewing (140 sec). The data were collected from 619 neurologically normal individuals, ages 18-87. The processed results from the resting recordings are completed and available for download at http://stash.osgconnect.net/+krieger/ . These constitute ≈1.7 TBytes of data including the location within the brain (1 mm resolution), time stamp (1 msec resolution), and 80 msec time course for each of 3.7 billion validated neuroelectric events, i.e. *mean* 6.1 million events for each of the 619 participants.**

The referee consensus solver provides high yield (*mean* 11,000 neuroelectric currents/sec; *standard deviation (sd)*: 3500/sec) high confidence (p < 10^{-12} for each identified current) measures of the neuroelectric currents whose magnetic fields are detected in the MEG recordings. We describe the solver, the implementation of the solver deployed on the Open Science Grid, the workflow management system, the opportunistic use of high performance computing (HPC) resources to add computing capacity to the Open Science Grid reserved for this project, and our initial findings from the recently completed processing of the resting recordings. This required ≈14 million core hours, i.e. ≈40 core hours per second of data.

Keywords—magnetoencephalography, MEG, referee consensus, opportunistic computing, shared data, concussion, TBI

I. INTRODUCTION

It has been the informed expectation for a century that the keys to understanding the human brain will be found in measuring and understanding the electrical activity of neurons. Today, clinical neurophysiologists routinely measure single neurons to aide implantation of therapeutic devices deep in the brain [5]. Epileptologists use arrays of implanted "stereo EEG" electrodes and the population recordings obtained from them to diagnose and guide the treatment of intractable seizure disorders [6].

It is population activity which is thought to be the basis for brain function. Stereo EEG and comparable invasive methods produce voltage recordings with resolution of a few millimeters at best from up to a few hundred recording sites. Because the electric field interacts strongly with the conducting tissue in the brain, these measures are difficult to localize if there is much tissue between the field source and the electrodes. This problem is particularly pronounced when the recordings are made noninvasively from electrodes placed on the scalp.
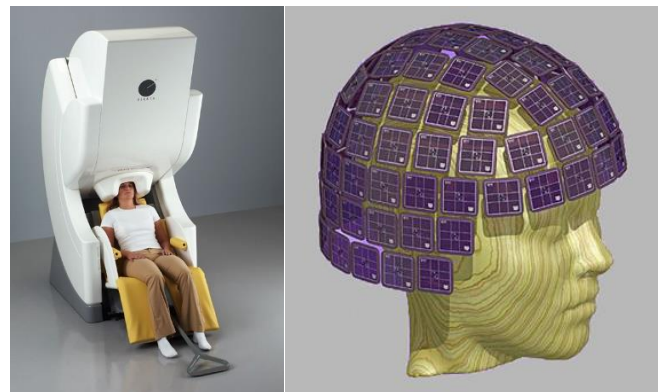

Fig 1. 306 channel whole head VectorView MEG scanner (Elekta, Inc., Stockholm, Sweden). The sensor array is composed of 102 planar "chips," each with 3 superconducting magnetic field sensors: one magnetometer, two figure-eight gradiometers at right angles to each other, and a superconducting quantum interference device (SQUID) coupled to each. The SQUID's are used to couple the minute currents induced by magnetic flux in the sensors to the room temperature electronics.

Magnetoencephalography (MEG) provides an alternative noninvasive measurement approach with several advantages over scalp and even implanted EEG recordings. A typical MEG scanner is shown in Figure 1. The magnetic fields produced by minute electric currents within the brain are measured at the MEG sensor array with high fidelity. Unlike electric fields, magnetic fields do not interact with brain tissue; they pass through it as if it weren't there. So in principle, the current which is the source of such a field is more readily localized. If the contribution to the MEG measurements of a single neuroelectric current source can be identified, the corresponding current can be accurately estimated using the Biot-Savart law [7].

The measurements at the MEG sensor array are due to an unknown and almost certainly large number of neuroelectric currents. The referee consensus method [8,9] enables reliable identification of one neuroelectric magnetic source at a time regardless of the number present. Since each identification is independent of all others, the method is readily ported to a loosely coupled supercomputing resource. We have deployed a solver based on this method to the Open Science Grid (OSG), a shared resource which supports research in many domains including particle and nuclear physics, computational chemistry, genomics and proteomics, and neuroscience.

II. METHODS: SOLVER IMPLEMENTATION AND RESERVED HIGH PERFORMANCE COMPUTING RESOURCES

The calculations are performed by a compiled and static linked executable. A single instance requires ≈300 Mbytes of memory and ≈35 Mbytes of disk space and network I/O. This network I/O is potentially a problem since the number of solver instances, i.e. jobs, required to process a single 560 second recording block is ≈75,000. This could require up to 2.6 TBytes of network I/O.

Two mechanisms are used to reduce this load. (A) For jobs run at-large on the OSG, data transfers are mediated by http servers which incorporate the SQUID data caching proxy[1]. This is effective because the data is identical for all jobs processing identical time segments, i.e. groups of ≈3000 jobs. Numerous spot checks show a consistent "hit" rate well above 95% which reduces the required data movement by more than 20:1. (B) For jobs which run on reserved glideins[2] on Comet[3] or Bridges, a single copy of the data is placed on the scratch disk of the machine for each group of ≈3000 jobs. An incremental copy operation is used, so if the file already exists on the disk, no network transmission is required.

CreateForward is a python script which generates the forward solution matrix, i.e. the map:

$$\text{neuroelectric current} \rightarrow \text{magnetic field} \,.$$

A single CreateForward instance with accompanying python package requires ≈400 Mbytes of memory and 20 Mbytes of disk space and network I/O. CreateForward is identical for all jobs. The SQUID file cache hit rate is near 100%. For reserved glideins on Bridges or Comet, this package is handled in the same way as is the data.

The shell scripts which manage the specialized portions of the workflow not readily handled by HTCondor[4] are detailed below in **Workflow Management**. At-large OSG jobs run opportunistically per HTCondor's fair-share algorithm [10]. Allocations were provided through XSede[5] on Comet and Bridges to add computing capacity for use on this project.

HTCondor's glidein mechanism is used to incorporate this added capacity directly into the OSG pool as reserved job slots. This enables use of the same workflow used for at-large jobs with almost no change and so minimized the software effort in utilizing these additional resources.

For processing the CamCAN data, we elected to run opportunistically on both Comet and Bridges in a way which insures that our glideins run only when there are idle cycles on the machines. In addition the glideins run for 2 hours only insuring that no job will wait on completion of our glideins for long. The performance of this system is illustrated in Figure 2. The dead time at the end of the short glidein lifespan during which new jobs starts are prohibited reduces job slot occupancy to 94%. Glideins with a 3-hour lifespan show 98% occupancy. The figure also shows the time required to burn through 5,000 core hours on Bridges "regular memory" nodes. For the rest of the 24-hour run shown, only "large memory" nodes were used.
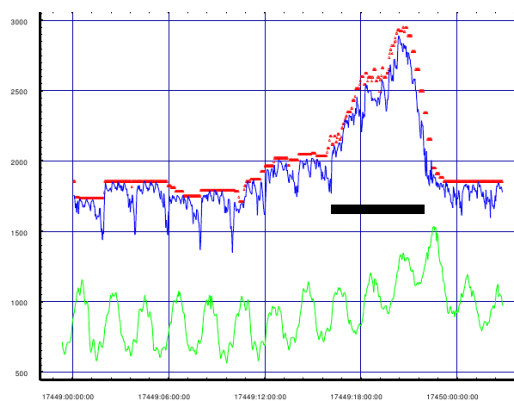

Fig 2. Bridges reserved jobs slots (red) and occupied jobs slots (blue) are shown for a 24-hour period. The black bar indicates a period during which 5000 "backfill" core-hours were used on regular memory nodes. Live versions of these figures may be found **here**.

The logic for this is implemented in a single script, *MonGlidein*. A single small group of glideins at a time is queued, 1 on Comet, 3 on Bridges. Each glidein uses either ½ or all of the cores on a single node. Only when no glideins are found waiting in the queue is a new group spawned. When a new group is spawned, *MonGlidein,* pauses for 30 seconds and checks to see if the group has begun running. If it has, a new group is spawned. If not the wait time is multiplied by 1.5. The wait time for polling is limited to 300 seconds. This algorithm has been robust and effective in productively utilizing idle cores on these machines for many months. Because the run time for each glidein is short, i.e. 2 hours, backfill cycles are effectively utilized, i.e. cycles on large groups of cores which must drain

---

[1] http://www.squid-cache.org/

[2] Glidein is a mechanism by which one or more grid resources (remote machines) temporarily join a local HTCondor pool. http://research.cs.wisc.edu/htcondor/manual/v7.6/5_4Glidein.html

[3] Comet and Bridges are high performance computers on which our effort has allocations. They are situated at the San Diego and Pittsburgh Supercomputing Centers respectively.

[4] HTCondor is the workflow management system which handles jobs submitted to the Open Science Grid. https://research.cs.wisc.edu/htcondor/

[5] Extreme Science and Engineering Development Environment.

for hours to accumulate the resources requested by large multi-node jobs.

III. METHODS: WORKFLOW MANAGEMENT

Shell scripts were developed to manage the workflow. This scripting effort was and is guided by several principles: (1) The workflow is conceived as a real-time problem. (2) The software pieces are each viewed as evolving prototypes [11]. In almost all cases, modifications have been introduced "on the fly" without disrupting the workflow. (3) Each script must be as lightweight as possible. Attention is particularly paid to minimizing use of shared resources, e.g. network and disk I/O. (4) As faults occur, the error conditions are identified and analyzed. The scripts are then modified to avoid or trap those error conditions, i.e. the software is progressively "bullet-proofed."

As is usually the case with supercomputing resources, access to the OSG is via a front-end node. In our case, this is a machine at Indiana University provided by XSede, *xd-login*. The solver processing pipeline begins with preprocessing the raw MEG files and uploading them to *xd-login;* it ends with the return of results files from *xd-login*. Both of these data movement operations are handled from the *master* node which is behind a firewall with no firewall exceptions required.

The parallelism inherent in the referee consensus method is due to the fact that one spatial location is tested for the presence of a neuroelectric current for one data segment at a time. Each search is independent of all others which freely enables separating searches both by time segment and by spatial location. In practice, one search is conducted per data segment for each 8x8x8 mm brain voxel. Fully covering the volume of the brain, ≈1.5 liter, requires ≈3,000 voxels.

The CamCAN resting data was collected in a single continuous 560 second sitting. This is divided into 25 time blocks; each solver instance searches one voxel for one of these time blocks. Hence ≈75,000 solver instances, i.e. jobs, are required to process one 560 second resting recording. These parameters were selected to limit the run length for each job to a *mean* of 850 sec. This *mean* runtime is long enough to run efficiently on the OSG and short enough to minimize the lost cycles due to idle job slots at the end of a 2-hour glidein run.

Each solver instance is spawned to run on a separate processor/core, i.e. each solver instance is a separate OSG job. These jobs are assembled and spawned by a script which runs on *xd-login*. A single *spawner* instance handles these functions for each group of five time segments for the ≈3000 voxels covering the whole brain. Hence five *spawners* are used for each 560 second resting recording, each of which handles ≈15,000 jobs. At the end of its run, each *spawner* spawns a *collector* script. The *collector* collects and sorts the results files and then sets a flag which is detected by the script on the *master* node which fetches the results.

There is a single *submaster* script running on *xd-login* which spawns the *spawners*. The *submaster* polls the HTcondor queueing system and provides job group completion information required by all *spawners* and *collectors*. Polling HTcondor for this information, a relatively heavyweight operation, is thereby confined to a single process which does so every 3 minutes. The *submaster* also controls the number of data blocks which have been uploaded to *xd-login* by the *master* node. It does so by setting a GO/STOP flag which is detected by the data preprocessing script which is running on the *master*.

This workflow management and spawning system works without interfering with other workflows with continuous *xd-login* throughput as high as 35,000 jobs for extended time periods. The system typically runs without fault for a month or more, i.e. from one *xd-login* reboot to the next.

IV. METHODS: HOW THE SOLVER WORKS

The magnetic field strength at each of the 306 MEG sensors is the weighted sum of an unknown but likely large number of magnetic fields. A few of these such as mains powerline signals may be identified and subtracted off , filtered out, or otherwise eliminated by standard signal processing methods. What remains is an unknown number of magnetic field signals, many of which are of significant interest. The challenge is to identify as many of these as possible, and to identify both the location and time course of the electric current which is their source. Hence, we have a deconvolution problem for which both the number, location, and time course of the contributors to our measurements are unknown.

Note that the nature of the problem as one requiring deconvolution may be ignored for data in which the magnetic field strength from a single current constitutes the great majority of the total measured field, e.g. very high amplitude epileptiform activity. This scenario can be forced by reducing the data to averaged MEG signals for which the time segments contributing to the average are time locked to a repeated event, e.g. a button press or stimulus presentation. This enhances the signal/noise of excursions in the waveforms which are time-locked to the sync point and so reduces the sensitivity of the processing method to non-sync'd signals. It also markedly attenuates high frequency activity and averaging "collapses" the data by the number of time segments that are averaged. These consequences of averaging typically reduce the quantity of information that can be extracted from the record by 100:1 or more.

In general, because the number of contributors to the measured field is unknown, it is not possible to solve the deconvolution problem directly, i.e. to find and characterize the complete set of electric currents whose magnetic fields account for the measurements. However one can write a set of equations which contain terms for a large number of putative neuroelectric currents whose locations cover the volume of the brain as densely as wished. For this approach, the number of unknown parameters is far larger than the number of measurements, i.e. the solution is "ill-posed." A unique and meaningful solution may still be found by introducing a regularization term and solving using a pseudo-inverse, e.g. MNE [12], sLoretta [13]. These approaches provide limited information as (1) they are susceptible to interference and (2) they have low spatial resolution.

An alternative approach is to construct a digital filter for each location within the brain whose activity is of interest, e.g. SAM [14]. This approach produces an estimate for the electric

current at a single location but that estimate is sensitive to sources found elsewhere which "leak through" the filter and contaminate it. This compromises both the spatial resolution and fidelity of the amplitude estimate. In addition, neither this method or the others provide a reliable and robust validation scheme.

The referee consensus method uses a large family of digital filters to test and validate the presence of one neuroelectric current at a time. A cost function and associated probability are computed which are robust enough to use 10^{-12} as the threshold p-value to accept a current at a specific location as a true source of a detectable magnetic field. These capabilities are used to conduct a search of the brain volume for one 80-msec data segment at a time as detailed below and in the appendix. The effectiveness of this scheme in rejecting false signals during noisy data epochs is shown in Figure 3.
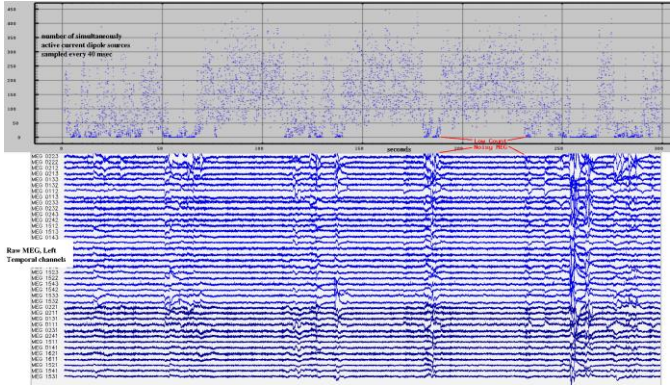

Fig 3: Neuroelectric source validation at $p < 10^{-12}$. The referee consensus solver automatically fails when the recordings are noisy. 300 seconds of raw MEG (lower) and neuroelectric currents (upper) are shown. The number of validated ($p < 10^{-12}$) currents identified drops markedly when the MEG is noisy.

Each data segment is a sequence of 80 observations in each of 306 magnetic field sensors. This may be considered as a vector with 80 x 306 = 24,048 components, i.e. as a point in a real space with 24,048 dimensions. The contribution to the magnetic field measurements at 306 sensors due to a dipole electric current at location **X** is the resultant magnetic field as it waxes and wanes over the 80 msec observation period.

The forward solution [15] which defines this relationship is nonlinear in the location parameters, xyz, but is linear in the amplitude. Hence the measured field due to the current at **X** is readily conceived as a point in $\mathscr{R}^{306} \times \mathscr{R}^{80}$, i.e. the Cartesian product of two real spaces with 306 (field shape) and 80 (amplitude time course) dimensions.

For a fixed **X**, the "shape" of the field is fixed, i.e. the ratios between each component of the field and every other is constant. Therefore the 80-point time course of the field measurement at each sensor is perfectly correlated or anti-correlated with that at every other sensor with the exception of sensors whose sensitivity is zero. That shape produces a set of 306 underlined values at the 306 magnetic field sensors, each of which is multiplied by an amplitude at each time point. Because the shape of the field is fixed, that shape multiplied by the amplitude always falls within a 1-dimensional subspace of $\mathscr{R}^{306}$, i.e. on a line within the space.

What is <u>unknown</u> is the 80-point time course of the current amplitude and the resultant 80-point time course of the magnetic field amplitude. It is the amplitude at each time point which determines where on the line in $\mathscr{R}^{306}$ the shape falls.

The 2-fold task of the solver is (1) provide a robust measure of confidence that a dipole current is detected at location **X** and (2) estimate the time course of the current amplitude. The method is briefly presented in the Appendix. It uses a family of digital filters which are highly tuned to the 1-dimensional subspace of $\mathscr{R}^{306}$ where the field due to a current at **X** falls and detuned to the orthogonal $\mathscr{R}^{305}$ subspace. Using this family of specialized filters produces a robust probabilistic measure of confidence that current is or is not present at **X** and a high fidelity estimate of the time course of the current when present.

V. Results

The referee consensus solver applied to MEG recordings isolates and identifies one localized neuroelectric current at a time, regardless of how many currents are simultaneously present. The solver is applied to the raw data stream one 80 millisecond (msec) time epoch at a time. For each time epoch, the total brain volume is searched for neuroelectric currents. In the control cohort resting data, a *mean* of 440, *sd* 130, simultaneously active currents were identified for each time epoch. The search progresses through the data stream in 40 msec steps, i.e. 25 steps per second, yielding about 11,000 neuroelectric currents per second, each validated at $p < 10^{-12}$. This threshold insures that almost all of the identified currents are real.

Here are several key characteristics of the neuroelectric current measures extracted from the MEG using the referee consensus solver. Note that the MEG is sampled at 1 KHz and filtered with high and low pass at 10 and 250 Hz, 5 Hz roll-off. Mains noise is removed at 50, 100, 150, 200, and 250 Hz. Continuous head positioning is recorded and used to correct the spatial localization once per second. Each identified neuroelectric current is an 80-point (80 msec) waveform localized with 1 mm resolution and validated at $p < 10^{-12}$. The frequency content of the identified waveforms is dominated by activity 20-150 Hz.

Note that those aged 18-65 were used to represent the portion of the CamCAN which matches our other cohorts. Hence the *n* is 414 rather than 619.

Approximately equal numbers of neuroelectric currents are identified in both gray and white matter. The unexpected detection of neuroelectric currents in the white matter and the high spatial resolution of their localization enables robust measures of gray vs white differential activation. Figure 4 shows a typical example from an individual in which differential activity, gray vs white, is seen with $p < 10^{-16}$ in several regions. Note that the gray matter region is more active than the white as expected in the right inferior parietal pair but the differential is reversed for the right rostral middle frontal regions.
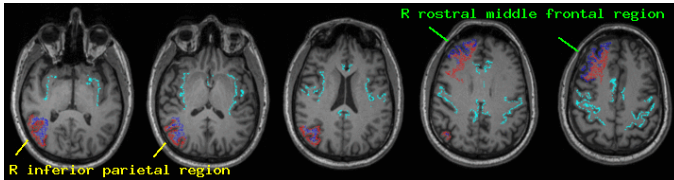
Fig 4. Activation is compared between the right inferior parietal cortex and the adjacent white matter (yellow marks) and between the right rostral middle frontal cortex and the adjacent white matter (green marks). The χ^2 statistic is computed for the difference between the densities. The fully saturated color indicates that the comparison is significant at $p < 10^{-16}$. For the parietal region the ROI shown in red, the cortex, is as expected, more active than the adjacent white matter, shown in blue. For the frontal region, the differential activation is the opposite, i.e. the adjacent white matter is more active than the cortex.

The 560 second CamCAN resting recordings produced a *mean* of 6.1 million (*sd* 1.9 million) localized and validated current estimates for each subject. These profuse, high resolution, highly reliable measures present a strikingly detailed and dynamic characterization of brain activity. The full set of results for the 619 members of this neurologically normal cohort represents an invaluable scientific resource. It contains measurements from 619 men and women, ages 18-87, providing age and sex matches for any adult population. The results have been placed online including the following:

(1) All validated neuroelectric sources for each member of the CamCAN cohort. Each source listing includes the xyz coordinates (1 mm resolution) of the source location, a time stamp (1 msec resolution), and the 80-point time course of the current amplitude.
(2) The output of the freesurfer run for each member of the cohort.
(3) The list of coordinates on a 1 mm grid which were searched for currents and the freesurfer region in which each location resides.
(4) A tool which is usable through the web browser to generate a complete list of download files for each member of the cohort. That list is designed to be used with wget to download the data.
(5) A tool usable on a linux machine with Intel or AMD processor which assembles the list of currents into simultaneously active groups and writes them to standard output as ascii characters. This need not be used since the data is already in compressed ascii form. But for many operations it will prove convenient.

Rather than pursuing analyses which capitalize on the high time resolution of our measures, our emphasis has been on the reliability of the measures. We use counting, i.e. the number of identified currents per unit volume as a measure of activity. We use freesurfer [16] to identify 164 standard brain regions of interest (ROI) and compute an activity density measure for each. The density measure is normalized both by the total counts[6] and total brain volume:

$$\rho_{ROI} = (count_{ROI}/count_{total})/(vol_{ROI}/vol_{total})$$

The counts are so large and the false identification rate is so low (e.g. Figure 4) that we have ample statistical power using the χ^2 statistic to identify differences between regional density measures, e.g. cortical region vs adjacent white matter region, region during rest vs the same region during task. The activity densities are reduced in deep structures and in the cerebellum. This is likely due to reduced sensitivity because these structures are further from the MEG sensor array. However, the numbers are ample even in the brainstem to see significant differential activation ($p < 10^{-4}$) when comparing rest and task.

Global patterns identified by standard eigenvector methods enable discrimination between the CamCAN cohort and those with chronic symptoms of concussion or with those at-risk for HIV with 100% accuracy (Figure 5). And the patterns themselves, also shown in the figure, are of significant interest.
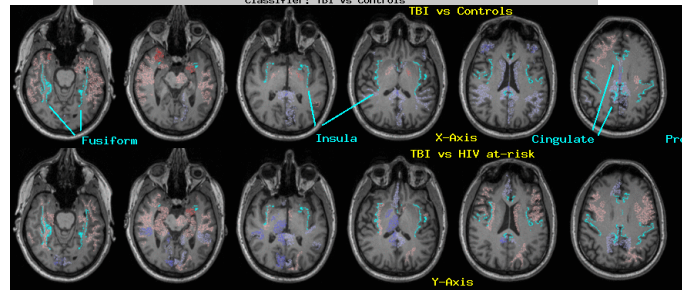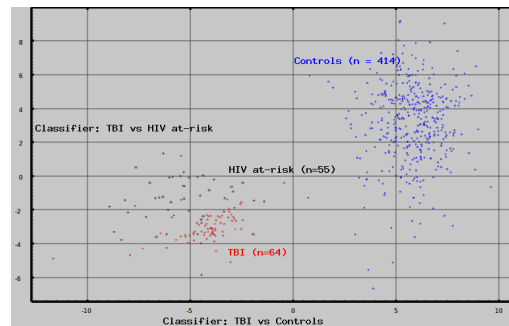

Fig 5: Regional patterns of brain activity[7] demonstrate high classification accuracy between cohorts. Neuroelectric activity density (ρ_{act}) was measured from resting MEG recordings in each of 164 brain regions in 3 experimental cohorts, (1) controls (n=414), (2) TBI (n=64), (3) HIV at-risk (n=55). The middle and lower panels show the brain regions which contribute their fair share or more to the classifier; Red/blue indicates a positive/negative weight, the more saturated (deeper) the color, the greater the weight. The cyan landmarks are the boundaries between gray and white matter in the pre-central, cingulate, insula, and fusiform regions.

We have also demonstrated a regional measure which provides network connectivity information. Instead of counting the number of neuroelectric currents which occur within a region, we count the number of pairs of simultaneously occurring currents for which one of the pair occurred within the region. Since we know the incidence over the recording session of each member of the pair, we can compute the chance that we

---

[6] Dividing the counts for a region by the total count normalizes the numerator of the "density" for variations due to regional volume, data quality and record length

[7] The first 20 independent components (ICAs) of these measurement vectors were identified from the control cohort. Each person's 164 measures were reduced to their factor scores on these 20 ICAs. Stepwise linear discriminant analysis (BMDP7M) was used on the factor scores to identify the best linear classifiers for one cohort from another. The classification accuracy for TBI vs controls was 100%; accuracy for TBI vs HIV at-risk was 76%.

would count the number of coincidences. We set a threshold of $p < 10^{-8}$ to accept a pair as occurring more often than expected. For the control cohort, we count a *mean* of 114,399 pairs for each 560 second resting recording, *sd* 80,492, *min* 8,328, *max* 563,220.

The number of such pairs with one member of the pair within a region and the other member outside the region provides a measure of the "coupling strength" of the region to the rest of the brain. The regional density is computed from this count in the same way as the activity density described above and, in fact, can be compared directly with it, i.e. the activity density of a region can be compared with its coupling strength.

Both the activity density and coupling strength measures provide enormous statistical power to test hypotheses about select brain regions in a single individual as shown in Figure 6. The figure shows differences between cortex and adjacent white matter for both activity and coupling measures for the entire CamCAN cohort. In addition, since the solver enables formal comparison of the activity densities of a cortical region with the adjacent white matter region. Under the plausible assumption that the rim of white matter largely terminates in the adjacent gray matter, the ratio of these densities, ρ_{ctx}/ρ_{wm}, is a measure of cortical excitability. This therefore provides a promising and previously inaccessible tool in addition to activity and coupling strength.
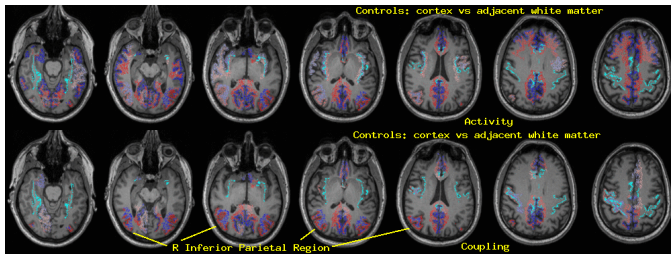

Fig 6: Regional differential activation/coupling, control cohort, cortex vs adjacent white matter. The average activity and coupling densities (see text) were computed for each of 164 regions for the control cohort (n=414). The mean for each cortical region was compared with the mean for the adjacent white matter region using Welch's t-statistic. Red/blue regions are more/less active (upper panel) or coupled (lower panel) than the adjacent region. The p-value for each regional comparison ranges from $p < 10^{-4}$ (light color) to $p < 10^{-8}$ (fully saturated color). Most of the regions which show differential activation show greater activation in the white matter than in the adjacent cortex. The right inferior parietal region is highlighted because its differential coupling strength is much more significant than its differential activation, despite the reduced statistical power in the coupling measure.

VI. DISCUSSION

This work is based on resource sharing and on the complementary principle, opportunism. The key elements of the work are shared, i.e. the CamCAN lifespan normative dataset, the Open Science Grid, the high performance computing resources, and the results of the work. Absent the data or the supercomputing resources to process it, the work could not go forward. Absent sharing the results, the value of the work is stunted since these results provide a characterization of the brain activity of a neurologically normal population with unprecedented detail. The availability of this dataset and the processed results provides controls to the wide community of workers using MEG to study both normal and pathological human brain function.

The emphasis of the work is methodological. The challenge is to use the measurements to advance our understanding of brain function both for research and for clinical purposes. The information extracted by the referee consensus solver provides unique opportunities to accomplish this.

(1) The individual neuroelectric currents are localized with millimeter precision. Their time course is measured with high fidelity in the frequency range: 12 – 250 Hz.
(2) Analysis of regional current density provides extraordinary statistical power in measuring differential regional activation, e.g. Figures 4 and 6.
(3) This approach demonstrates the capability of the solver to reliably identify neuroelectric currents within the brain's white matter, e.g. Figure 4. Aside from a few recent results in the fMRI literature [17], this is the only known method which produces detailed functional measures from this critically important and previously inaccessible portion of the brain.
(4) The robust detection of differential activation between a cortical region and the adjacent white matter rim and the fact that it is often the white matter which shows greater current density suggests that it is synchronous volleys of action potentials which are at the basis of the currents detected by the solver. This conclusion is supported by the predominance of high frequency content in the identified waveforms.
(5) The adjacent rims of white matter paired with cortical regions by freesurfer are at most 5 mm thick. They include the thin layer of white matter extending into the cortical gyri and separating the cortex on one side of the gyrus from the other. Under the assumption that the majority of the fibers in each white matter region terminate in the adjacent cortex, we propose the ratio of the activity in a cortical region with the adjacent white matter as a measure of cortical excitability.
(6) Analysis of regional activity using standard dimensional reduction methods, i.e. eigenvector analysis, produces physiologically interpretable patterns which distinguish between groups with very high accuracy, e.g. Figure 5, and which are highly correlated with a variety of pathological symptoms. The identified patterns provide one dimensional axes within the very high dimensional space of brain states with a defined direction toward "normal."
(7) Analysis of groups of simultaneously active currents provides remarkable statistical power to detail the coupling strength, i.e. functional connectivity, between one brain volume and the rest of the brain, e.g. Figure 6.
(8) Analysis of the regional current density over time provides a means to extend the utility of these processed results to study low frequency phenomena. The presumed interpretation of the extracted current waveforms as representative of synchronous volleys of action potentials ties this analysis directly to the underlying neurophysiology.

Transcranial magnetic stimulation (TMS) [18] applied to select brain regions is a promising treatment modality. This safe and painless device has been used successfully in patients with major depression and obsessive compulsive disorder. The activity and coupling measures described here will likely be

sensitive to treatment with TMS. Hence these measures might be used to monitor changes in brain activity in those undergoing this treatment. Since measures on our large control cohort nominally provide the direction of asymptomatic, if we can understand and predict how TMS effects brain activity, these measures could potentially be used to guide treatment with TMS.

REFERENCES

[1] JR Taylor, NWilliams, R Cusack, T Auer, MA Shafto, M Dixon, LK Tyler, Cam-CAN, RN Henson, "The Cambridge Centre for Ageing and Neuroscience (Cam-CAN) data repository: Structural and functional MRI, MEG, and cognitive data from a corss-sectional adult lifespan sample," Neuroimage 144: 262-269, 2015, PDF.

[2] MA Shafto, LK Tyler, M Dixon, JR Taylor, JB Rowe, R Cusack, AJ Calder, WD Marslen-Wilson, J Duncan, T Dalgleish, RN Henson, C Brayne, CamCAN, FE Matthews, "The Cambridge Centre for Ageing and Neuroscience (CamCAN) study protocol: a cross-sectional, lifespan, multidisciplinary examination of healthy cognitive ageing. BMC Neurology 14(204), 2014, PDF.

[3] R Pordes, D Petravick, B Kramer, D Olson, M Livny, A Roy, P Avery, K Blackburn, T Wenaus, F Wurthwein, "The open science grid," J Physics 78, 2008, PDF.

[4] I Sfiligoi, DC Bradley, B Holzman, P Mhashilkar, S Padhi, F. Wurthwein, "The pilot way to grid resources using glideinWMS," WIR World Cong Comp Sci and Info Engg 2: 428-432, 2009, PDF.

[5] I Telkes, J Jimenez-Shahed, A Viswanathan, A Abosch, N Ince, "Prediction of STN-DBS electrode implantation track in Parkinson's Disease by using local field potentials," Front. Neurosci 10: 1-16, 2016, PDF.

[6] F Moroni, L Nobili, G Curcio, F De Carli, F Fratello, C Marzano, L De Gennaro, F Ferrillo, M Cossu, S Francione, G Lo Russo, M Bertini, M Ferrara, "Sleep in the human hippocampus: a stereo-EEG study," PLoS One 2(9): e867, 12Sep2007, PDF.

[7] J Sarvas, "Basic mathematical and electromagnetic concepts of the biomagnetic inverse problem," Phys. Med. Biol. 32(1): 11-22, 1987, PDF.

[8] D Krieger, M McNeil, J Zhang, W. Schneider, X Li, DO Okonkwo, "Referee consensus: a platform technology for nonlinear optimization," XSEDE 2013, ACM 978-1-4503-2170-9/13/07, PDF.

[9] D Krieger, M McNeil, J Zhang, A Puccio, W Schneider, X Li, DO Okonkwo, "Very high resolution neuroelectric brain imaging by referee consensus processing," Intl. J. Advd. Comp. Sci. (4)1: 15-25. Jan 2014, PDF.

[10] B Jayatilaka, T Levshina, M Rynge, C Sehgal, M Slyz, "The OSG open facility: A sharing ecosystem," J Phys: Conf Ser. 664 PDF .

[11] M Deutsch, "Software Quality Engineering: A Total Technical and Management Approach," Prentice-Hall, Englewood Cliffs, NJ, 1988.

[12] MS Hamalainen, RJ Ilmoniemi, "Interpreting magnetic fields of the brain: minimum norm estimates," Med. and Biol. Engg and Compg 32(1): 35-42, 1994, PDF.

[13] RD Pascual Marqui, CM Michel, D Lehmann, "Low-resolution electromagnetic tomography – a new method for localizing electrical activity in the brain," Intl J Psychophys 18(1): 49-65, 1994, PDF.

[14] J Vrba, SE Robinson, "Signal processing in magnetoencephalography," Methods 25: 249-271, 2001, PDF.

[15] J Sarvas, "Basic mathematical and electromagnetic concepts of the biomagnetic inverse problem," Phys. Med. Biol. 32(1): 11-22, 1987, PDF.

[16] B Fischl, M Sereno, A Dale, "Cortical surface-based analysis," NeuroImage 9: 195-207, 1999, PDF.

[17] T Warbrick, J Rosenberg, NJ Shah, "The relationship between BOLD fMRI response and the underlying white matter as measured by fractional anisotropy (FA): a systematic review," NeuroImage 153: 369-381, 2017, PDF.

[18] M Eid, Y Qanir, "Evidence based practice: transcranial magnetic stimulation for major depression," Intl. J. Psych. Br. Sci. 1(1): 13-20, 2016, PDF.

APPENDIX

The 2-fold task of the solver is (1) provide a robust measure of confidence that a dipole current is detected at location $\mathbf{X}$ and (2) estimate the time course of the current amplitude

The solver is applied to one 80 msec data segment ($\mathbf{M}_{t=1,...,80}$) at a time. A decision is made for one location at a time, e.g.: "Is there a dipole current present at location $\mathbf{X}$?" To answer this question, spatial filters are constructed from the "viewpoints" for each of 90 distant "referee" locations distributed widely through the volume of the brain, e.g. $\mathbf{R}$.

Filter $\mathbf{P_{R!X'}}$ is constructed with gain 1.0 at $\mathbf{R}$ and gain 0.0 at $\mathbf{X'}$ 1 mm from $\mathbf{X}$. $\mathbf{P_{R!X'}}$ is applied to the 80 data vectors, $\mathbf{M}_{t=1,...,80}$, to produce the 80-point univariate time series, $\mathbf{V_{R!X'}}$. A 2nd filter is constructed, $\mathbf{P_{R!X}}$, with gain 1.0 at $\mathbf{R}$ and gain 0.0 at $\mathbf{X}$. $\mathbf{P_{R!X}}$ is also applied to $\mathbf{M}_{t=1,...,80}$ to produce the 80-point univariate time series, $\mathbf{V_{R!X}}$. Note that there is a small contribution to $\mathbf{V_{R!X'}}$ from activity at $\mathbf{X}$ but none from $\mathbf{X'}$. Contrariwise there is a small contribution to $\mathbf{V_{R!X}}$ from activity at $\mathbf{X'}$ but none from $\mathbf{X}$.

The difference filter is constructed, $\mathbf{P_{R!X'-R!X}}$. This has gain 0.0 at $\mathbf{R}$ and nearly equal and opposite gains at $\mathbf{X}$ and $\mathbf{X'}$. $\mathbf{P_{R!X'-R!X}}$ applied to $\mathbf{M}_{t=1,...,80}$ produces $\mathbf{V_{R!X'-R!X}}$, the difference: $\mathbf{V_{R!X'}} - \mathbf{V_{R!X}}$. Note that there is no contribution to this from $\mathbf{R}$. Note too that each of these 3 filters is constructed with gain 0.0 at each of 89 other "referee" locations coarsely covering the brain so $\mathbf{V_{R!X'-R!X}}$ includes only small contributions from other neuroelectric currents. This insures that the primary contributors to $\mathbf{V_{R!X'}}$ - $\mathbf{V_{R!X}}$ are currents close to $\mathbf{X}$ and/or $\mathbf{X'}$.

The "opinion" from the viewpoint of referee $\mathbf{R}$ regards the presence of a current at $\mathbf{X}$ is obtained by evaluating this inequality:

$$(\mathbf{V_{R!X'-R!X}} \bullet \mathbf{V_{R!X'}})^2 > (\mathbf{V_{R!X'-R!X}} \bullet \mathbf{V_{R!X}})^2 \qquad (1)$$

If the inequality is true, then there is a current at $\mathbf{X}$ from the viewpoint of $\mathbf{R}$ since $\mathbf{V_{R!X'}}$ (left side) has no contribution from $\mathbf{X'}$, $\mathbf{V_{R!X}}$ (right side) has none from $\mathbf{X}$, and $\mathbf{V_{R!X'-R!X}}$ has nearly equal contributions from both.

This procedure is repeated for each of the 90 referee locations to produce 90 yes/no "opinions." 57 or more must be "yes" (p < 0.01) to produce an acceptable "consensus" for this differential. The same procedure is repeated for each of the

other 5 differentials since there are two differentials along each of the 3 spatial axes. Only if all 6 exceed the threshold, i.e. 57 or more of 90 for each of the 6, is a current accepted. $0.01^6 = 10^{-12}$ is therefore the threshold for accepting a current.

Once a location is validated, an eigenvector analysis is used to identify the 80-point time course of the current at that location as the waveform which captures the most variance in the complete set of $\mathbf{V_{R!X'-R!X}}$'s. Note that the validation insures that there is a current present at $\mathbf{X}$ and not at any of the six $\mathbf{X}$'s. Hence the primary contributor to all of the $\mathbf{V_{R!X'-R!X}}$'s is due to the current at $\mathbf{X}$.